The Astrophysical Journal, 671:581–591, 2007 December 10

SEISMOLOGY OF PRE-MAIN-SEQUENCE STARS IN NGC 6530[1]

D. B. Guenther
Department of Astronomy and Physics, Saint Mary's University, Halifax, NS B3H 3C3, Canada

T. Kallinger, K. Zwintz, and W. W. Weiss
Institut für Astronomie, Universität Wien, Türkenschanzstrasse 17, A-1180 Wien, Austria

and

J. Tanner
Department of Astronomy and Physics, Saint Mary's University, Halifax, NS B3H 3C3, Canada
Received 2007 May 30; accepted 2007 August 21

ABSTRACT

Nonradial *p*-mode oscillation spectra, computed from a dense grid of pre-main-sequence models, are fit to observed oscillation spectra of several stars in the young cluster NGC 6530. The five stars we consider, all previously identified as pulsating pre-main-sequence stars, each have from two to nine observed oscillation frequencies. For those stars with a more complete set of frequencies we are able to constrain the models using the oscillation spectra alone and confirm that the stars are in their pre-main-sequence and not post-main-sequence phase of evolution. For the stars with only two observed frequencies we are able to reduce the solution space of possible models. Comparing our model fits to the surface temperatures and luminosities derived from the observed colors and parallaxes, we find that the model fits are consistent with the cluster's distance, i.e., the luminosities agree, but we discover that all of our models are systematically too cool. We attribute some of the discrepancy in the surface temperature to uncertainties in the surface boundary conditions of our models, but argue that most of the difference is a direct consequence of applying a single average color-dependent dereddening correction to all the stars when, in fact, it appears that the stars we selected are embedded in varying degrees of gas and dust. For one of the stars we identify a rotationally split $l = 1$ *p*-mode from which we derive a rotation period of 18 days.

Subject headings: δ Scuti — stars: evolution — stars: oscillations — stars: pre–main-sequence — stars: variables: other

1. INTRODUCTION

When a young star with more than about 1.5 $M_{\odot}$ evolves off the Hayashi track (Hayashi 1961) toward the zero-age main sequence (ZAMS), where nuclear burning replaces gravitational collapse as the dominant source of power (Iben 1965), it passes through the classical instability strip. Over two dozen pre-main-sequence (PMS) stars in this region of the H-R diagram have been specifically identified as pulsating variables (e.g., Breger 1972; Kurtz & Marang 1995; Donati et al. 1997; Marconi et al. 2000; Zwintz et al. 2005). Some of these PMS stars reveal oscillation spectra containing more than one mode, and some of the modes, as our models show, could be nonradial *p*-modes (Zwintz et al. 2007, hereafter ZGW07).

By comparing the observed oscillation spectra of these stars to models we are able to determine the nature of the oscillations and test the correctness of the models. This is especially useful because accurate effective temperatures and luminosities, with which the models are constrained, are often not available for young stars that are still enshrouded in the gas and dust from which they were formed. For pulsating PMS stars located within a cluster, asteroseismology can help confirm cluster membership and provide an independent age and distance estimate for the cluster. By fitting models to the observed oscillation spectrum we can determine the mass, age, luminosity, and effective temperature of the star. It is important to note, however, that the model solutions do depend on the physics of the models and, in particular, on the assumed helium abundance and the mixing-length parameter. Both the helium abundance and mixing-length parameter are determined from calibrated models of the Sun.

Since the interiors of PMS stars are not yet stratified into regions of processed nuclear material nor, it is believed, complicated by strong rotation gradients, they should be much easier to model than, for example, the δ Scuti stars that also occupy this region of the H-R diagram. Most δ Scuti stars are post-main-sequence stars passing through the instability strip on their way toward the giant branch. They exhibit complex oscillation spectra, including mode bumping and rotational splitting, that have proven to be very difficult to model.

The first efforts to fit models to the oscillation spectra of PMS stars are encouraging. Zwintz et al. (2005) were able to find radial-mode fits to some of the frequencies in some of the PMS stars they observed. They speculated that the unmatched modes could be nonradial modes. This led to the more detailed modeling attempt by ZGW07 for one of the stars in NGC 6383. They were able to fit the star's observed location in the H-R diagram and all five of the observed frequencies with a single model and its corresponding *nonradial p*-mode oscillation spectrum.

In preparation for results from COROT (Baglin et al. 2002), Ruoppo et al. (2007) reviewed some basic strategies of PMS model and oscillation spectra fitting. As a demonstration of their methodology they found tentative nonradial oscillation model fits to V351 Ori and IP Per.

In this work we examine five stars believed to be PMS stars belonging to the young star cluster NGC 6530. We assume that all the stars are at a common distance and have similar compositions and young ages. The cluster was specifically chosen because

[1] Based on observations with the 0.9 m telescope at the Cerro Tololo Inter-American Observatory, La Serena, Chile.

the PMS pulsating stars associated with the cluster have from a couple to almost a dozen observed modes, thereby enabling us to study how effective the oscillation spectra are at constraining the models as a function of the number of observed modes. The selected group of stars in NGC 6530 are embedded to varying degrees in the gas and dust of the Lagoon Nebula (M8); hence, uncertainties in the dereddening corrections are expected.

We use the observational results and numbering of Zwintz & Weiss (2006), who observed NGC 6530 in 2002 August using the 0.9 m telescope at Cerro Tololo Inter-American Observatory in Chile. The cluster was observed using the 2048×2046 SITe CCD chip over 12 of 14 nights, yielding a total of 80.16 hr of photometric data. The reader is referred to Zwintz & Weiss (2006), where the observations and reduction methodology are described in detail.

2. MODEL GRID

We have found that the most effective strategy to model the sparse nonradial oscillation spectra observed in stars is to search through dense and extensive grids of model spectra looking for the best match to the observed spectrum as quantified by a χ^2 measure of the quality of the fit. The models within our grids span a range of mass and age, with each grid itself characterized by a specific composition and mixing-length parameter. The methodology was originally developed by one of us (see Guenther & Brown 2004) to address the difficulties in matching the observed oscillation spectra of stars in more advanced phases of evolution where mode bumping introduces irregularities in the approximately equally spaced distribution of individual mode frequencies of consecutive radial order. The search and spectrum-matching strategy was adapted from the earlier work of Fontaine that studied the oscillation spectra of hot subdwarfs (Brassard et al. 2001; Charpinet et al. 2005). Applications to post-main-sequence stars can be found for α Cen A (Guenther & Brown 2004), η Boo (Guenther et al. 2005, 2007), and Procyon (Guenther et al. 2007). The method was also used to model the oscillation spectrum of a PMS star in NGC 6383 (ZGW07).

The grids of models used here (three PMS and one post-main-sequence) were constructed using the Yale Stellar Evolution Code (YREC; Guenther et al. 1992). PMS models were evolved from the Hayashi track (Hayashi 1961) to the ZAMS. The grids include models with masses ranging from 0.810 to 4.99 $M_\odot$ in steps of 0.01 $M_\odot$. Each evolutionary track is resolved into approximately 1000 models for a total of ~400,000 models in each grid.

The physics of the models are current and include OPAL98 (Iglesias & Rogers 1996), the Alexander & Ferguson (1994) opacity tables, and the Lawrence Livermore National Laboratory equation of state tables (Rogers 1986; Rogers et al. 1996). The mixing-length parameter, an adjustable parameter which sets the temperature gradient in convective regions according to the Böhm-Vitense (1958) mixing-length theory, was set from calibrated solar models constructed using the same input physics. As an aside we note that the actual value of the mixing-length parameter needed to produce a model of the Sun with the observed radius and luminosity at the age of the Sun depends sensitively on the surface boundary conditions, the atmosphere model, the low-temperature opacities, and whether or not helium and heavy-element diffusion is included. Different stellar evolution codes, even when using similar physics, will require different values for the mixing-length parameter owing to minor differences in their numerics, such as interpolation schemes. It is important for consistency, therefore, to not just adopt a number for the mixing-length parameter but to determine it for the code in use from a calibrated model of the Sun. Nuclear reaction cross sections are from Bahcall et al. (2001). Our PMS tracks compare well with the tracks of D'Antona & Mazzitelli (1994), and our post-main-sequence tracks are identical to the standard reference tracks of the Yonsei-Yale group (Yi et al. 2003).

We begin our models on the Hayashi track before deuterium burning, and not on the birth line (Stahler 1983) as do the reference models of Palla & Stahler (1992, 1993). Because the birth line depends sensitively on the mass-loss rate (Palla & Stahler 1992), which our models do not include, we decided at this stage of our investigations to focus on more accessible parameters of the models. When we have a better feeling for the capability and reliability of our model fits to PMS stars, we will return and examine the timescales of PMS evolution more carefully.

The model pulsation spectra were computed using Guenther's nonradial nonadiabatic stellar pulsation program (Guenther 2004). The code uses the Henyey relaxation method to solve the linearized nonradial nonadiabatic pulsation equations. The nonadiabatic component includes radiative energy gains and losses as formulated in the Eddington approximation but does not include coupling of convection to the oscillations (see Balmforth 1992; Houdek et al. 1999). All oscillation spectra fits presented here were carried out with the adiabatic frequencies.

The quality of the match is quantified by the simple χ^2 relation,

$$\chi^2 \equiv \frac{1}{N} \sum_{i=1}^{N} \frac{\left(\nu_{\mathrm{obs},i} - \nu_{\mathrm{mod},i}\right)^2}{\sigma_{\mathrm{obs},i}^2 + \sigma_{\mathrm{mod},i}^2},$$

where $\nu_{\mathrm{obs},i}$ and $\nu_{\mathrm{mod},i}$ are the observed frequency and the corresponding model frequency for the ith mode, respectively, $\sigma_{\mathrm{obs},i}$ and $\sigma_{\mathrm{mod},i}$ are the corresponding uncertainties, and N is the total number of matched modes. The model uncertainties are estimated from solar-model fits (Guenther & Brown 2004). For the observations considered here they are an order of magnitude smaller than the observational uncertainties, hence, negligible.

For each star we search the grid of oscillation spectra looking for models for which $\chi^2 \leq 1$. When χ^2 is less than 1, the difference between each of the observed frequencies and the corresponding nearest model frequency (only counted once) is less than the rms of the model and observational uncertainties. In the special case here where the model uncertainties are negligible, models with $\chi^2 \leq 1$ correspond to fits in which all the model frequencies lie within the observational uncertainties of the observed frequencies.

Because we do not have any knowledge of the degrees of the modes, we normally carry out an initial search restricted to radial modes within the grid. This step is especially useful when modeling post-main-sequence stars, owing to the effects of mode bumping on the nonradial modes. We note that for post-main-sequence models the grid resolution needs to be at least 10 times greater in age and mass in order to resolve smoothly the effects of mode bumping. For PMS stars we still find it helpful to look for and identify the radial modes first to see where ambiguities in mode identification might occur. Once we have a feeling for which modes could be radial modes we repeat the search but allow nonradial modes to be considered in the match. Normally, with a well-matched spectrum the identity of the matched modes does not change when we include higher degree nonradial modes in the search.

Although we are specifically looking for $\chi^2 < 1$, we note that because χ^2 depends on our estimate of the uncertainties, if our uncertainty estimates are too low or too high then our χ^2 values will also be too low or too high. We discuss this further in § 3.6 for star 278 in NGC 6530.

We also look for smooth variations in χ^2 and well-defined minima as a function of model parameters. In our tests of the search and mode-matching software we found that spurious frequencies cause χ^2 to vary randomly or chaotically as functions of the model parameters such as mass and age. This is because the searching algorithm tries to find fits to all the modes so that sometimes the errant mode will be fit and sometimes not. For these errant spectra χ^2 does not smoothly drop to a minimum as a function of, for example, age.

For one of the stars (star 278) we also compared its oscillation spectrum to our grid of post-main-sequence stars. Although we do not doubt the young age of the cluster, we perform this test to show that the oscillation spectra can be used to test the overall evolutionary state of individual stars, thereby helping confirm their cluster membership. The grids are identical in mass coverage, except that they correspond to models evolved from the ZAMS to the giant branch.

3. PMS STARS IN NGC 6530

3.1. *Introduction*

NGC 6530 is a young stellar cluster located in the central regions of the Lagoon Nebula. The distance to the cluster is well known, 1.86 ± 0.07 kpc (McCall et al. 1990). The cluster is believed to be from 1 to 3 Myr old (Kilambi 1977; Sung et al. 2000).

In the following subsections we describe each star in turn, beginning with stars for which only a couple of frequencies are observed, and ending with two stars having more than a half-dozen frequencies each. As we increase the number of modes, predictably, our ability to constrain the model fits improves. When the results for all the stars are considered as a group, we find model fits consistent with the presumed luminosity based on the cluster's distance modulus but systematically too cool when compared to the dereddened color temperatures. This, we argue, is due to the varying amounts of gas and dust surrounding the stars.

In Figure 1 we show the observed positions of the stars in an H-R diagram along with several PMS evolutionary tracks selected from our model grid. All of the stars, as selected by Zwintz, lie within the red and blue boundaries of the instability strip (Zwintz et al. 2005), consistent with the fact that they are observed to oscillate. Note, however, that not all the stars observed by Zwintz that lie within the instability strip have detectable oscillations.

In Figure 2 we show the locations of the stars within the cluster itself. The Digitized Sky Survey image shows the two fields observed by Zwintz. Blue contours mark edges of equal intensity. Here we draw attention to the variation in the intensity of the gas and dust emission near the stars. We also note that the stars are located in relatively low intensity regions compared to the very center of the nebula.

In Table 1 we summarize the observed H-R diagram properties of the stars as taken from Zwintz (2006). Table 1 also lists the mass, surface temperature, luminosity, and surface gravity ($\mathrm{m\,s^{-2}}$) of the models that best fit the observed oscillations (discussed below). The observed oscillation frequencies in units of microhertz are listed in Table 2 for each star. The observations for star 85 that were reanalyzed with more current data reduction software are also listed (see § 3.4).

3.2. *Star 5* (*WEBDA 159*)

The grid search program calculates χ^2 for each model in the grid, storing oscillation and model details for models with low

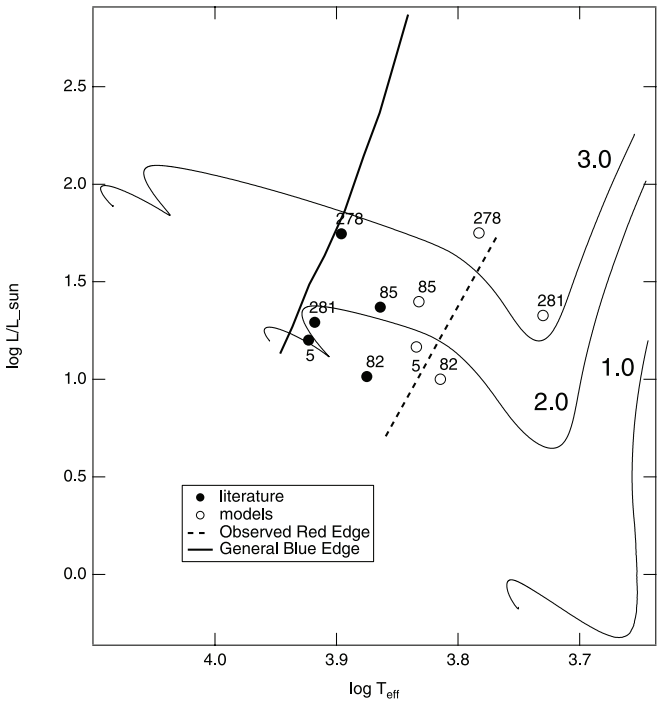

FIG. 1.—H-R diagram showing the positions of five PMS stars in NGC 6530. Filled circles correspond to published values, and open circles correspond to models that best fit the *p*-mode oscillation spectra. The red and blue edges of the post-main-sequence instability strip are also shown.

χ^2. In Figure 3 we show only those models that have adiabatic *p*-mode oscillation spectra that match the two observed frequencies with $\chi^2 \leq 1$. We present the results of two searches, one where we assume the two observed modes are purely radial, and the other where we allow a mix of $l = 0$ (radial) and $l = 1$ modes. When we assume the frequencies are purely radial modes, the solution set of models is more restricted. In order to find models that match the oscillations and also lie within the observational uncertainties in the H-R diagram location of the star, we must assume that the modes are radial and nonradial; i.e., we cannot find a purely radial oscillation spectrum solution consistent with the observations.

With only two frequencies to constrain the models it is not possible to say much more, although we do consider it significant that with only two modes we have constrained the number of possible models to the stringlike regions within the H-R diagram.

In order to understand why the solutions lie along diagonal lines, consider first how the oscillation spectra are matched. To first order the matching of the observed oscillation spectrum to the models is determined primarily by the spacing of the modes. This applies to all stellar oscillation spectra, not just star 5. The observed frequencies will be fit not only by models that have similar spacings between adjacent modes, but also by models that have the same mode spacings between alternate modes. In general, any commensurable combination of mode sequences can be matched. Another way of saying this is that we do not know the *l*- or *n*-values of the observed frequencies. They could be a sequence of radial modes, they could be a sequence of only odd *n*-valued radial modes, they could be a sequence of $l = 0$ and 1 modes, or they could be some other combination. The corresponding characteristic spacing (i.e., the asymptotic spacing between modes adjacent in *n*) of the spectrum will be different for each case. Because the approximately regular spacing between modes is known from asymptotic theory (Tassoul 1980) to

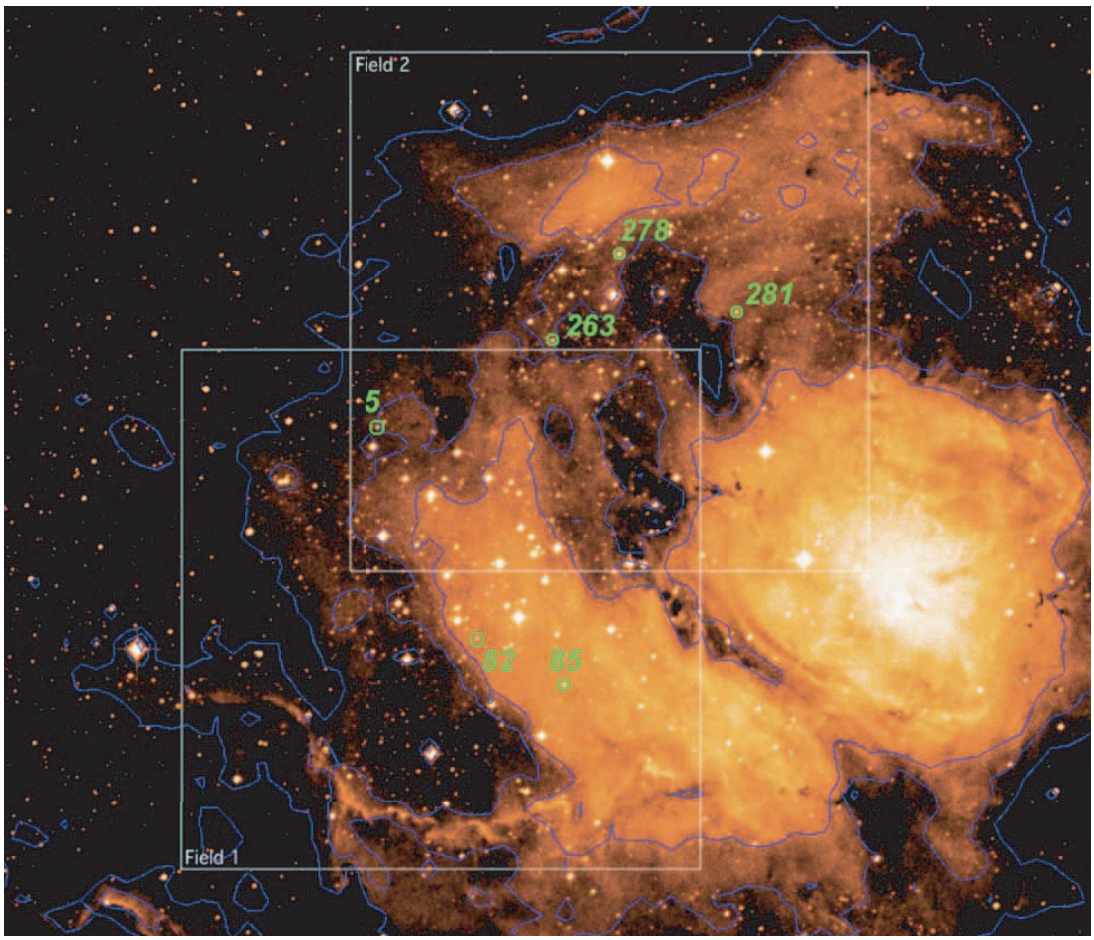

FIG. 2.—Two observed fields and the locations of the discussed PMS stars in NGC 6530. Scattered light emission from the Lagoon Nebula (M8) dominates the image.

depend on the sound travel time through the star, for a given mass the models that fit the observed oscillation spectrum should have roughly the same mean density on which the sound travel time depends. This is what we see in our solutions. The model fits lie along diagonal lines in the H-R diagram that define models with approximately similar sound travel times. The different lines of model fits correspond to different combinations of mode spacing sequences, hence, different characteristic spacing and, correspondingly, different mean densities.

The radial order of the two $l = 0$ modes of our best-fit model that match the observed frequencies are $n = 13$ and 15.

Our nonadiabatic pulsation code calculation of the modes for the best radial model fit shows that both modes are driven. The real oscillation modes are also subject to gains and losses from stochastic interactions with the turbulent fluid motions within the convective envelope, and these effects, which may be as important as radiative effects (Balmforth 1992), are not accounted for in our nonadiabatic calculation.

3.3. *Star 82* (*WEBDA 78*)

There are three observed frequencies available to constrain models for star 82. If we assume all the frequencies are radial modes, we obtain only a few possible model solutions, all in a region, labeled "A" in Figure 4, more luminous and cooler than the observed H-R diagram position. Allowing $l = 1$ modes to be included in the fit produces a wider range of possible solutions, including some models, labeled "B" in Figure 4, at the observed luminosity but still cooler than implied by the color temperature for star 82.

The nonadiabatic pulsation code calculation of the modes for the best nonradial model fit shows that the lowest frequency

TABLE 1
OBSERVATIONAL AND BEST-FIT MODEL SUMMARY FOR NGC 6530

	Literature		Model				
Star	$\log T_{\rm eff}$	$\log L/L_\odot$	Mass ($M_\odot$)	$\log T_{\rm eff}$	$\log L/L_\odot$	g	χ^2
5	3.923	1.20	1.87	3.834	1.17	67	0.115
82	3.875	1.01	1.72	3.815	1.00	77	0.677
85	3.864	1.37	2.27	3.832	1.40	47	0.974
278	3.896	1.75	3.53	3.783	1.75	21	0.077
281	3.918	1.29	3.28	3.730	1.33	31	0.215

TABLE 2
OBSERVED MODES

Mode	Star 5	Star 82	Star 85	Star 85 Updated	Star 278	Star 281
P1	539.31	287.37	122.51	122.58	48.36	355.22
P2	618.25	401.28		133.38	69.59	433.53
P3		445.96	146.99	147.02	83.33	442.65
P4				167.47	109.81	463.16
P5			179.76	179.65	138.70	467.21
P6			180.31	180.26	140.29	482.66
P7				180.95	152.99	502.52
P8				327.31	160.83	
P9			360.51	360.48	181.53	

NOTE.—Frequencies are in microhertz.

mode is driven ($l = 1$, $n = 5$), and the other two modes ($l = 0$, $n = 7$ and 9) are damped.

3.4. *Star 85* (*WEBDA 53*)

For star 85 in NGC 6530 Zwintz has identified five frequencies, although two of them, at 179.76 and 180.31 μHz, are very close together, and as we show below are likely to be part of a rotationally split mode. Indeed, the existence of a possible rotationally split mode motivated us to recheck the data analysis for this star using our latest algorithms. Doing so not only resolved the mode at 180 μHz into a triplet, but also revealed three additional frequencies. Note that rechecking the frequencies of the other stars confirmed the original observations but did not reveal any new frequencies.

With the original five frequencies we are able to find model fits over a relatively restricted solution space, as shown in Figure 5. Fits were obtained for four of the five frequencies, with the models fitting either the 180.31 or the 179.76 μHz mode, but not both simultaneously. The fits were to $l = 0$ and 1 p-modes. The frequencies could not be fit with radial modes alone. There is one model that lies at the edge of the uncertainty range for star 85's H-R diagram position (labeled "A" in Fig. 5) and a small string of models lying above and to the right of this (labeled "B"). The best-fitting model, A, has the correct luminosity but lies at the cool side of the uncertainty range in surface temperature.

In Figure 6 we show, in an echelle diagram (frequency vs. frequency modulo 27 μHz), the $l = 0$, 1, and 2 p-modes of the best-fitting model (model A in Fig. 5), along with the five originally detected frequencies shown as open circles (open squares represent frequencies from the updated analysis of the observations described below). The radial orders n of some of the modes are also labeled. For reference a complete list of the model frequencies is provided in Table 3. The observational uncertainty, corresponding to one over the duration time for the observations, is approximately ± 0.5 μHz and is smaller than the plot symbols. We discuss the observational uncertainty in § 3.6 for

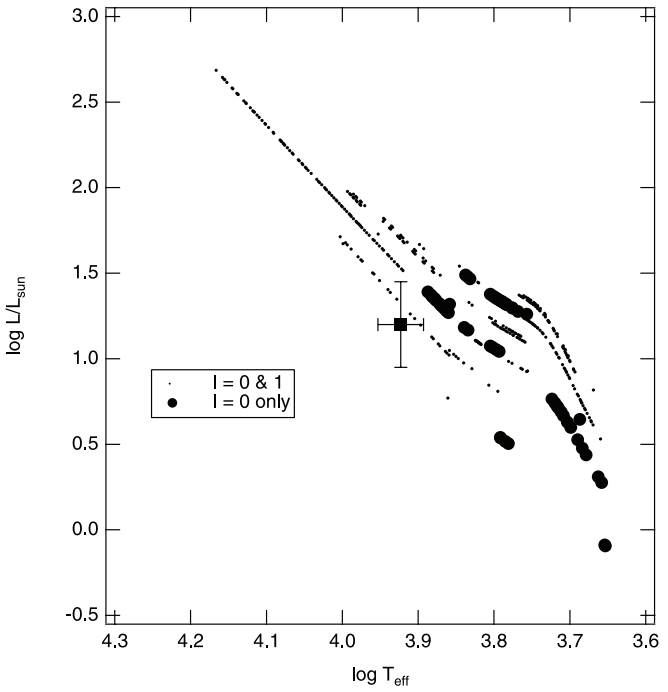

FIG. 3.—H-R diagram showing the location of the models that fit the two observed frequencies with $\chi^2 \leq 1$ for star 5 in NGC 6530 and the location of star 5 based on luminosity and temperature derived from *Hipparcos* parallax and photometry.

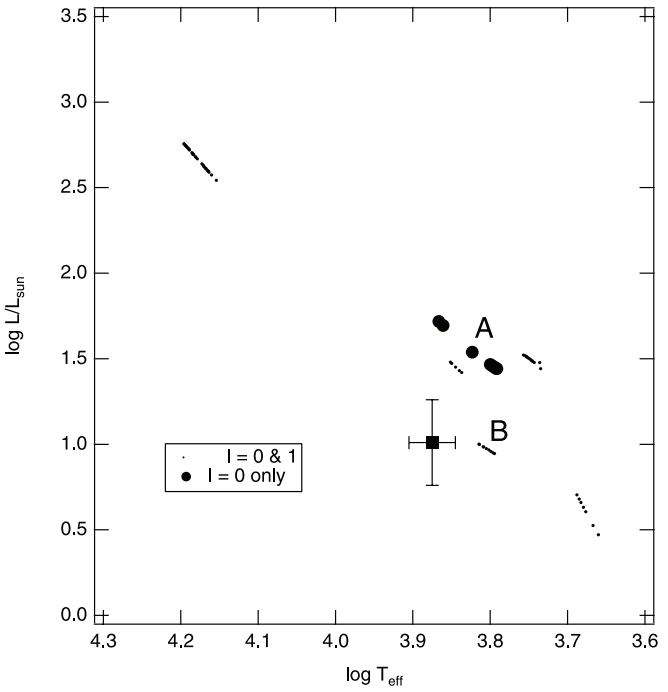

FIG. 4.—H-R diagram showing the location of the models that fit the three observed frequencies with $\chi^2 \leq 1$ for star 82 in NGC 6530 and the location of star 82 based on luminosity and temperature derived from *Hipparcos* parallax and photometry.

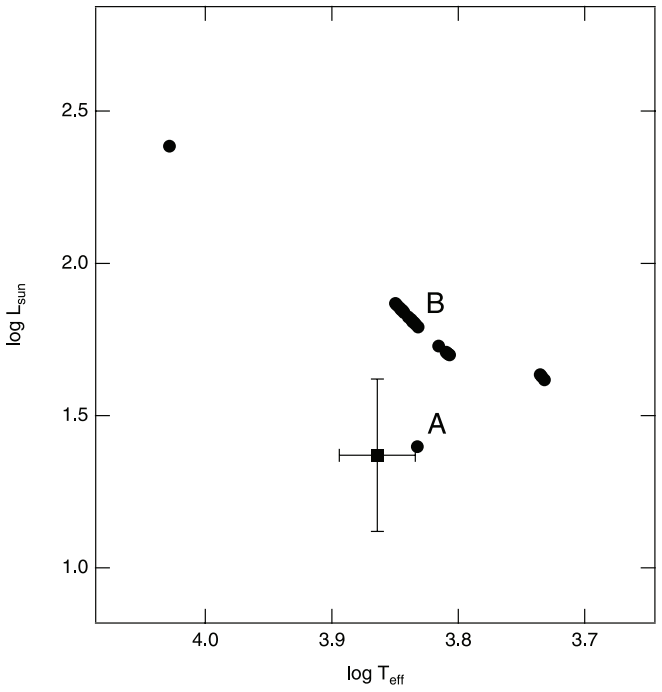

FIG. 5.—H-R diagram showing the location of the models that fit the five observed frequencies with $\chi^2 \leq 1$ for star 85 in NGC 6530 and the location of star 85 based on luminosity and temperature derived from *Hipparcos* parallax and photometry.

star 278, since it appears that our uncertainty estimate may be too pessimistic.

Remarkably, with just four frequencies observed over a period of approximately 2 weeks, one can restrict the solution space to a small region in the H-R diagram. We found only one model

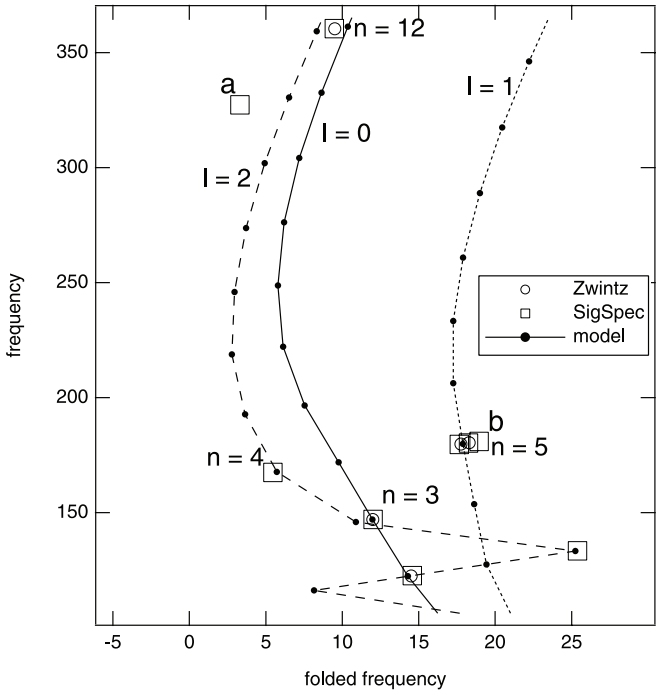

FIG. 6.—Echelle diagram with a folding frequency of 27 μHz showing the $l = 0$, 1 and 2 p-modes for the best model fit, "A" in Fig. 5, to the observed frequencies for star 85 in NGC 6530. The frequencies derived originally by Zwintz are depicted with open circles, and those from the reanalyzed data (SigSpec; Reegen 2007) are shown with open squares.

TABLE 3
STAR 85: ADIABATIC MODEL FREQUENCIES

n	$l = 0$	$l = 1$	$l = 2$	$l = 3$
0	76.1	86.3	102.4	116.9
1	98.2	102.3	116.2	124.5
2	122.3	127.4	133.2	146.6
3	147.0	153.6	145.9	154.4
4	171.8	...	167.7	175.7
5	196.5	179.9	192.6	201.7
6	222.1	206.3	218.8	228.6
7	248.8	233.3	245.9	256.3
8	276.2	260.9	273.7	284.5
9	...	289.0	301.9	313.0
10	304.2	317.5	330.5	341.8
11	332.6	346.2	359.3	370.8
12	361.4	375.2	388.3	399.9
13	390.3	404.2	417.3	428.9
14	419.3	433.2	446.2	457.9
15	448.2	462.1	475.1	486.7
16	477.0	490.8	503.8	515.4
17	505.8	519.5	532.4	544.0
18	534.4	548.1	561.0	572.7
19	563.0	576.8	589.7	601.5
20	591.8	605.6	618.7	630.6
21	620.8	634.8	647.9	659.9
22	650.1	664.1	677.3	689.4

NOTE.—Frequencies are in microhertz.

within 1 σ of both the oscillation observations and the observed position in the H-R diagram. This solution would have been easily missed if the grid resolution in mass were coarser than $\sim$0.01 $M_{\odot}$.

Because of the existence of a possible rotationally split mode and the good model fit already obtained, we were curious to see what our latest reduction software would reveal in the original observations. We reprocessed the original time series data in the same manner as described in Zwintz & Weiss (2006) but with better frequency analysis using SigSpec (Reegen 2007). This improved the robustness of the results, and hence gave us greater confidence in the mode identifications at lower amplitudes. We selected frequencies with spectral significance greater than 10. Note that a spectral significance equal to $\sim$5.5 corresponds to a signal-to-noise ratio of 4 (Reegen 2007). The newly identified frequencies are, therefore, still above the generally adopted signal-to-noise ratio limit of 4 also used by Zwintz et al. (2005). With the reanalysis we identified three additional modes and resolved the two modes near 180 μHz into a triplet. In Figure 6 we plot, with open squares, the nine significant frequencies obtained from the reanalyzed observations. Only the new frequency at 327 μHz ("a" in Fig. 6) is not fit by any of the $l = 0$, 1, or 2 p-modes of the model.

The newly analyzed data reveal a triplet for the model-identified $l = 1$ p-mode at 180 μHz ("b" in Fig. 6). The triplet is seen in the B band observations (see Fig. 7), and the high-frequency component as a 1 day^{-1} alias in the V-band observations. The separations $\Delta f1$ and $\Delta f2$ are 0.61 ± 0.08 and 0.675 ± 0.16 μHz, respectively, corresponding to an average splitting of 0.643 ± 0.09 μHz. Assuming this triplet is due to rotation (consistent with it being an $l = 1$ p-mode) and the star is rotating as a solid body, the rotation period is 18.0 ± 0.25 days. Using the radius of the best-fit model gives a $v \sin i$ of less than $\sim$10 km s^{-1}. This is a relatively slow rotation rate, and hence would make the star a good candidate for spectroscopic observations to study, for example, element abundances.

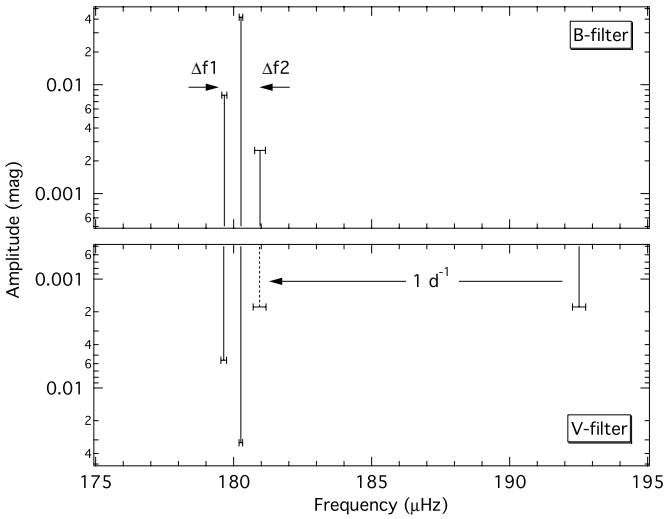

FIG. 7.—Amplitude of the triplet "b" in Fig. 6 vs. frequency in *B*- and *V*-band filters. The high-frequency mode of the triplet in the *V* band appears as a 1 day^{-1} alias.

The nonadiabatic pulsation code calculation of the modes for the best model fit (labeled "A" in Fig. 5) shows that all of the observed frequencies are driven.

3.5. *Star 281* (*WEBDA 13*)

For star 281 we are able to fit six of the seven frequencies observed by Zwintz (see Fig. 8) with $\chi^2 \leq 1$ using $l = 0$ and 1 p-modes. The large plot symbols in Figure 8 show $\chi^2 \leq 0.25$. Through some trial and error we found that in order to obtain low χ^2 we had to remove the frequency at 467.21 μHz. Our searching software, when looking for the best match to the observed spectrum, considers the possibility that one or more of the observed modes are unmatchable for a given model (Guenther & Brown 2004).

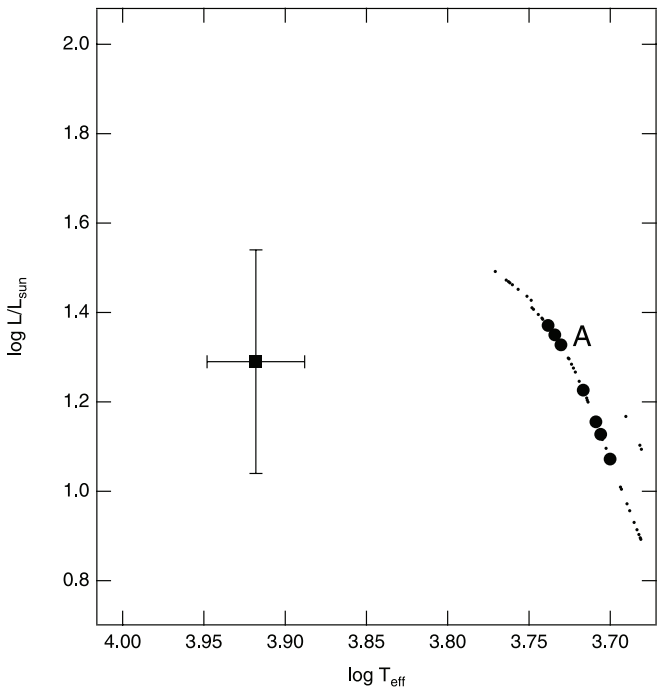

FIG. 8.—H-R diagram showing the location of the models that fit six of the seven observed frequencies with $\chi^2 \leq 1$ for star 281 in NGC 6530 and the location of star 281 based on luminosity and temperature derived from *Hipparcos* parallax and photometry. The large plot symbols correspond to model fits to the oscillation spectrum with $\chi^2 \leq 0.25$.

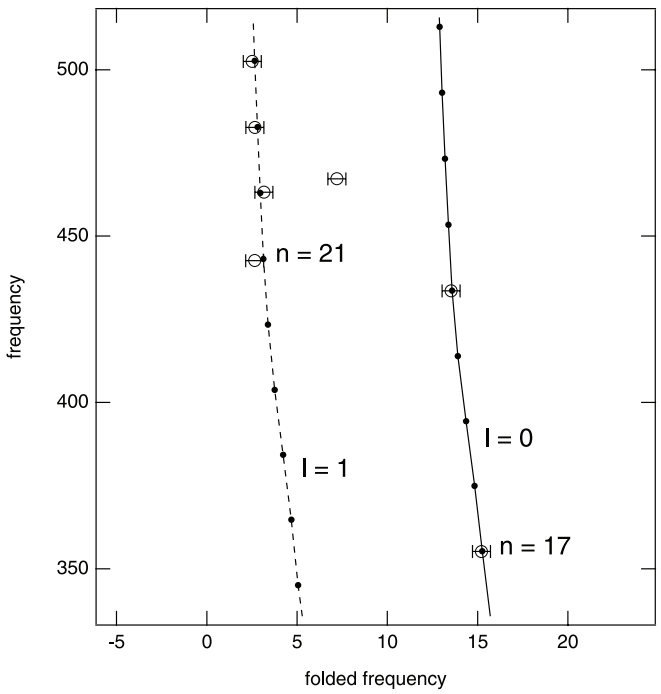

FIG. 9.—Echelle diagram with a folding frequency of 20 μHz showing the $l = 0$ and 1 p-modes for the best model fit, "A" in Fig. 8, to the observed frequencies (*large open circles*) for star 281 in NGC 6530.

As an aside, we note that if more than one or two modes cannot be matched for any model, then the task of finding the best model becomes more complicated and the results more ambiguous. When we suspect that the observed spectrum contains several nonstellar frequencies, we first search for best-fit models near the star's H-R diagram position and try to identify just the radial p-modes. Again restricted to the star's location in the H-R diagram, we next look for $l = 1$, then $l = 2$, and finally $l = 3$ p-modes, each time expanding our list of matched modes and, at the same time, identifying modes that systematically resist fitting. The process depends on restricting the solution space to be near the star's location in the H-R diagram; otherwise, wildly different combinations of realistic versus anomalous mode identifications are possible. Our experience has shown that when it comes to fitting models to the oscillation spectrum, it is extremely important to know with certainty that the peaks in the observed oscillation spectrum are of stellar origin.

The model fits to the six frequencies are confined to a long string of models, all of which are located at lower surface temperatures than the H-R diagram position of star 281. Indeed, the best-fitting model for star 281 lies outside the instability strip (see Fig. 1). The model oscillation spectrum of the best-fitting model (labeled "A" in Fig. 8) does, however, match well the observed spectrum, as shown in the echelle diagram in Figure 9. The frequencies and their n- and l-values for the best-fitting model are listed in Table 4.

The nonadiabatic pulsation code calculation of the modes for the best model fit shows that all of the modes are damped. This is consistent with the fact the best model fit lies outside the instability strip. At this time we do not consider that the location of this star beyond the red edge of the instability strip invalidates our solution. Stochastic excitation may also play an important role in the driving of oscillations in this region of the H-R diagram. For example, for post-main-sequence stars, we know that

TABLE 4
STAR 281: ADIABATIC MODEL FREQUENCIES

n	$l = 0$	$l = 1$	$l = 2$	$l = 3$
0	33.5	...	32.5	35.3
1	54.0	39.6	50.2	57.6
2	...	63.7	73.2	80.7
3	75.9	85.7	95.2	103.1
4	97.7	107.6	116.6	124.5
5	118.8	128.7	137.8	145.7
6	139.9	149.6	158.6	166.8
7	160.7	170.6	179.5	187.5
8	181.5	191.0	199.6	207.4
9	201.5	210.6	218.8	226.4
10	220.6	229.5	237.9	245.8
11	239.7	248.9	257.5	265.7
12	259.3	268.7	277.4	285.4
13	279.1	288.3	296.9	304.9
14	298.6	307.7	316.3	324.4
15	317.9	327.1	335.9	344.2
16	337.5	346.8	355.8	364.3
17	357.4	366.9	375.9	384.4
18	377.4	386.9	395.9	404.4
19	397.4	406.9	415.9	424.4
20	417.3	426.8	435.8	444.5
21	437.2	446.8	455.9	464.6
22	457.3	466.9	476.1	484.9
23	477.4	487.1	496.3	505.2
24	497.6	507.3	516.5	525.4

NOTE.—Frequencies are in microhertz.

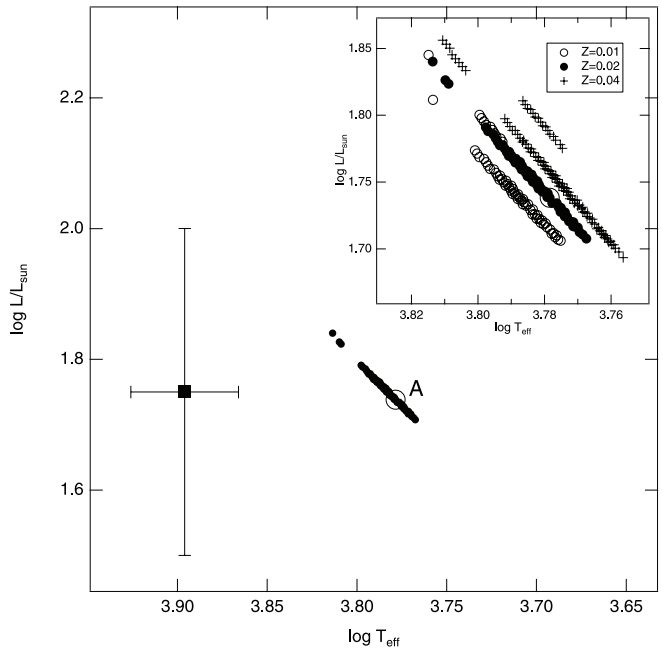

FIG. 10.—H-R diagram showing the location of the models that fit eight of the nine observed frequencies with $\chi^2 \leq 1$ for star 278 in NGC 6530 and the location of star 278 based on luminosity and temperature derived from *Hipparcos* parallax and photometry. The inset shows the effect of lower ($Z = 0.01$) and higher ($Z = 0.04$) metallicity on the solution space.

subgiants, e.g., α UMa (Buzasi et al. 1999), which occupy the same region of the H-R diagram, exhibit low-amplitude *p*-mode oscillations.

3.6. *Star 278* (*WEBDA 38*)

Zwintz identified nine frequencies in star 278, of which we are able to fit all but the lowest frequency at 48.36 μHz with $l = 0$, 1, and 2 *p*-modes. The $\chi^2 \leq 1$ solution space is shown in Figure 10. The best model fit with $\chi^2 = 0.077$ is circled (labeled "A" in Fig. 10). Note that the low χ^2 could indicate that our estimate of the uncertainties is too large by at least a factor of approximately 3. Indeed, Zwintz (2006) quotes much lower uncertainties in the frequencies than the commonly assumed one over the observation duration used here, based on a more sophisticated error estimate formula from Montgomery & O'Donoghue (1999) that scales the rms magnitude of the data set by the inverse square root of the number of data points, the inverse of the amplitude, and the inverse of the observation duration. Specifically, we take the uncertainty to be ± 0.5 μHz, while the Montgomery formulation yields a much smaller frequency uncertainty of ± 0.02 μHz. The Montgomery formula assumes the mode amplitudes are constant, i.e., that the modes have infinite lifetimes. If the mode amplitudes vary over the observing run, then the frequencies of the modes obtained by a Fourier transform (which assumes constant amplitudes) will be smeared out. We expect that the true frequency uncertainties will lie somewhere in between these two estimates.

The solution space is well constrained to a small string of models to the right of the observed H-R diagram position of the star. Again, as with all previous solutions, we find that our best-fitting models lie at the luminosity of the star but at a lower surface temperature. For star 278, with eight of the nine frequencies fit, it seems unlikely that our model fit is fortuitous, especially when the models do lie at the correct luminosity. We are therefore increasingly suspicious of the effective temperatures, both those predicted by our models and those inferred by the observations. That is, we wonder whether or not our models have the correct surface boundary conditions, and we wonder whether or not the surface temperatures deduced from the color indices are correct.

Figure 11, an echelle diagram, shows how well the *p*-modes of the best model match the observed frequencies. This fit provides our strongest evidence for the existence of nonradial modes in PMS stars. The frequencies and their *n*- and *l*-values for the best-fitting model are listed in Table 5.

We have assumed that our stars are indeed PMS stars. In the case of star 278 the observed oscillation spectrum is complete enough to enable us to discriminate between PMS and post-main-sequence stars. Post-main-sequence stars will have a more centrally concentrated interior, a consequence of nuclear burning occurring in the cores of these stars; hence, stars of similar luminosity and radius will have slightly different small spacings (Suran et al. 2001; Tanner 2006). Since star 278 appears to have $l = 0$, 1, and 2 *p*-modes, it is a good candidate to see if *p*-modes alone can differentiate between PMS and post-main-sequence evolutionary phases.

Using the eight matched modes we searched our post-main-sequence model grid in a manner identical to that for our PMS model grid. Both grids have the same composition (i.e., solar) and assume the same mixing-length parameter (i.e., calibrated to a solar model). In Figure 12 we show χ^2 versus surface temperature results from both searches side by side. The PMS solutions shown in Figure 11 correspond to the PMS models with $\chi^2 \leq 1$ in Figure 12, i.e., those models near $\log T_{\rm eff} = 3.77$. No post-main-sequence model fits the oscillation frequencies with $\chi^2 \leq 1$, and indeed, the best model fit corresponds to only $\chi^2 \simeq 5$. Because we cannot find a model fit to the observed oscillation spectrum from our grid of post-main-sequence models, and because

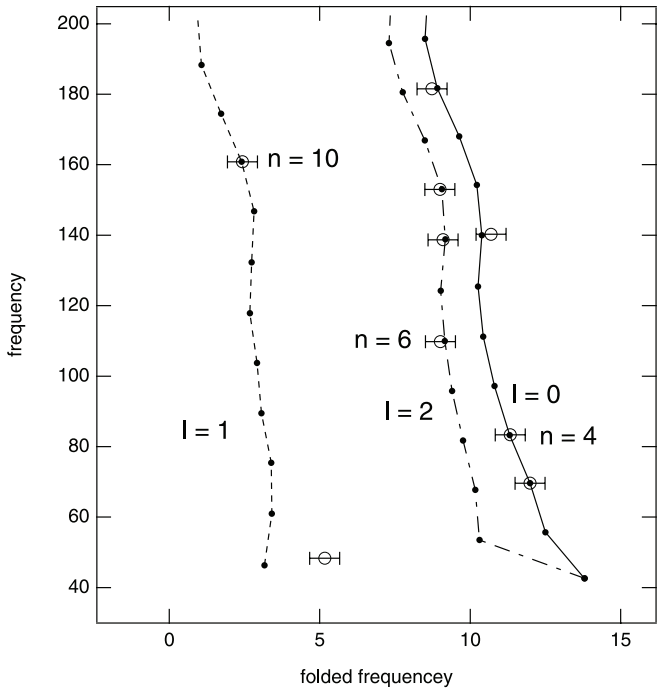

FIG. 11.—Echelle diagram with a folding frequency of 14.4 μHz showing the $l = 0$, 1, and 2 p-modes for the best model fit, "A" in Fig. 10, to the observed frequencies (*large open circles*) for star 278 in NGC 6530.

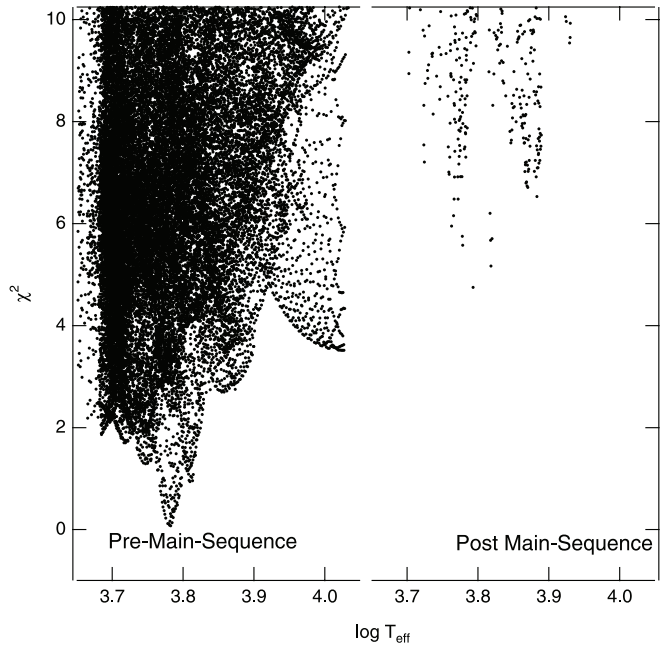

FIG. 12.—Measure of the quality of fit, χ^2, between the observed and model oscillation spectra of star 278 vs. log $T_{\rm eff}$ for a grid of PMS stars on the left and a grid of post-main-sequence stars on the right.

we can find models that fit the oscillations from our PMS grid, we conclude, based on asteroseismic data, that star 278 is a PMS star.

Returning to the discrepancy in surface temperature between the observed and oscillation model fit values, we consider the possibility that the metal abundance of the star (hence, also the cluster) is not solar. When using a grid of PMS stars with $Z = 0.01$ and 0.04, we found our $\chi^2 \leq 1$ model solutions to lie at slightly hotter and cooler surface temperatures, respectively, in the H-R diagram, as shown in the inset to Figure 10. The magnitude of the shift, however, is not large, and certainly not large enough to resolve the surface temperature discrepancy.

It remains possible that adjustments to the mixing-length parameter, currently calibrated to a standard solar model, could resolve the discrepancy. This would be an unexpected result that would have a significant impact on all PMS model calculations. Since we are focusing on the conclusions that can be drawn from standard modeling assumptions, we will return to this subject, if motivated by confirming observations, at a future date.

The nonadiabatic pulsation code calculation of the modes for the best model fit shows that all of the observed $l = 0$ and 1 modes are driven and the $l = 2$ modes are damped.

TABLE 5

STAR 278: ADIABATIC MODEL FREQUENCIES

n	$l = 0$	$l = 1$	$l = 2$	$l = 3$
0	32.0	33.4	37.7	42.4
1	42.6	46.4	42.6	45.9
2	55.7	...	53.5	57.9
3	69.6	61.0	67.8	72.6
4	83.3	75.4	81.8	86.8
5	...	89.5	95.8	101.1
6	97.2	103.7	110.0	115.3
7	111.2	117.9	124.2	129.8
8	125.5	132.3	138.8	144.4
9	140.0	146.8	153.1	158.5
10	154.2	160.8	166.9	172.3
11	168.0	174.5	180.6	186.0
12	181.7	188.3	194.5	200.3
13	195.7	202.5	209.0	214.9
14	210.2	217.1	223.6	229.5
15	224.8	231.7	238.2	244.1
16	239.4	246.3	252.6	258.5
17	253.8	260.6	266.9	272.8
18	268.1	274.9	281.3	287.2
19	282.4	289.3	295.7	301.7
20	296.9	303.8	310.3	316.4
21	311.5	318.4	325.0	331.1
22	326.2	333.2	339.7	345.8

NOTE.—Frequencies are in microhertz.

4. DISCUSSION

In Figure 1, in addition to the observed location in the H-R diagram of the PMS stars discussed above, we plot the model-derived locations of the stars. In the case of stars 5 and 82 we use the $\chi^2 \leq 1$ model that was closest to the observed luminosity, as shown in Figures 3 and 4, respectively. For the other stars we took the model with the minimum χ^2. The model results are also summarized in Table 1. Compared to the observed H-R diagram positions, the models are all located at cooler surface temperatures. The luminosities of the model PMS stars with minimum χ^2 all lie within the uncertainties of the observed luminosities.

If we assume that all of the stars are members of the cluster, then the models constrained by only the oscillation observations support the independently derived distance to the cluster. But at the same time, the models imply that the color temperatures of the stars are wrong, the surface temperatures of the model fits are wrong, or both.

It seems to us unlikely that the surface temperatures of our best-fit models for the PMS stars are all wrong to such a large extent. First, we note that the differences vary among the models yet are uncorrelated with their mass or position in the H-R diagram,

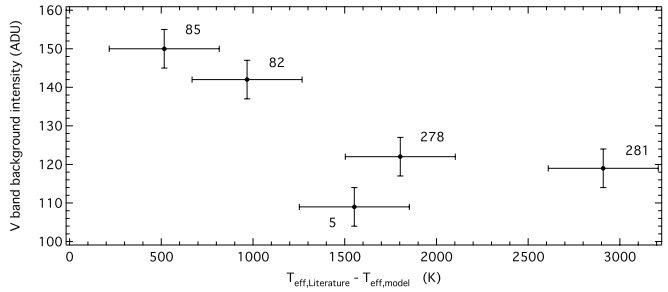

FIG. 13.—*V*-band filter background intensity vs. the difference between the published surface temperature and the surface temperature of the best-fitting models.

that is to say, there does not appear to be an obvious model dependency for the discrepancy. Second, the PMS evolutionary tracks themselves, from which the oscillation spectra are derived, are consistent with the published results of others. Third, the stellar evolution and pulsation codes are well tested on other stars and, for example, produce the expected results for the PMS star in NGC 6383.

As we noted in the introduction, the stars in NGC 6530 are embedded in gas and dust. It is our conjecture that the stars were dereddened to excess when their color temperatures were derived. Average color-dependent dereddening values were applied to the stars based on corrections determined near the center of the Lagoon Nebula. To support this, we note that the amount of gas and dust next to each star correlates linearly with the difference between model and observed surface temperatures. In Figure 13 we plot the *V*-filter background intensity opposite the temperature difference. The stars with the greatest temperature difference correspond to stars surrounded by the least amount of gas and dust as quantified by the amount of scattered light in their vicinity. Assuming that all the stars were dereddened using an amount more appropriate for stars located deep within the nebula, then the PMS stars studied here, located away from the center of the nebula, would be overcorrected. As a consequence, they would appear to be too blue, i.e., too hot. The stars that are embedded the least would have been overcorrected the most.

We are not too concerned that star 5 does not fit the linear relation. Recall that star 5 has only two observed frequencies; hence, there is considerably greater ambiguity in the best model fits. The two frequencies could be nonradial modes, and this would lead to a different best-fit model.

In order to constrain the distance to a cluster of stars using the observed oscillation frequencies of its cluster members, it appears that one needs at least approximately six frequencies per star (e.g., stars 281 and 287) observed to an accuracy of ± 0.5 μHz. Conversely, if the distance to the cluster is known, as in the case of NGC 6530, then the inferred luminosity of the individual stars can be used to help remove the ambiguities in the mode identifications.

5. SUMMARY AND CONCLUSIONS

We modeled the oscillation spectra of five PMS stars observed in the young cluster NGC 6530. The stars themselves each have from two to nine individual frequencies. Even with only two frequencies to constrain the models, we are able to reduce significantly the set of possible models. For star 278, with nine observed frequencies, we were able to reduce the solution set of models to a small enough region in the H-R diagram to confirm the observed luminosity of the star (and, correspondingly, the distance to the cluster). The small solution space also revealed that the previously derived color temperatures of this and the other stars may be too hot to varying degrees.

The discrepancies between our model temperatures and the observed color temperatures do not correlate with mass or H-R diagram position. They do, however, correlate with the amount of scattered light from gas and dust in the vicinity of the star. We speculate that the PMS stars studied here, which lie outside the center of the Lagoon Nebula within which they are embedded, have all been dereddened to varying degrees of excess.

In order to match all the observed oscillation spectra seen in the stars, with the exception of star 5, for which only two modes were observed, we had to include nonradial *p*-modes ($l \leq 3$) in our fits.

For star 85 we identify a mode triplet, which, when interpreted as a rotationally split $l = 1$ *p*-mode, yields a rotation rate of 18 days, assuming solid-body rotation.

For star 278, for which nine frequencies are observed to an accuracy of ± 0.5 μHz, we show that the oscillation spectrum can only be fit (with $\chi^2 \leq 1$) by PMS models and not post-main-sequence models ($\chi^2 \geq 5$). The oscillation spectrum was fit by $l = 0$, 1, and 2 *p*-modes.

We show that the effect of metal abundance, although measurable, does not significantly affect the H-R diagram positions of the models that match the oscillation spectra.

Our models, if accepted, imply that some PMS stars located in the region to the right of the red edge of the classical instability strip in the H-R diagram can oscillate (stars 82 and 281). We do not know what the driving mechanism could be for stars in this region, but speculate that, like their post-main-sequence counterparts, they are driven by stochastic interactions with turbulent motions in the outer convective envelope. We support efforts to observe pulsating PMS stars in this region of the H-R diagram, since we are not aware of any well-constrained (by observations) PMS stars in this region of the H-R diagram that are known to pulsate. Note that in order to increase her probability of detecting pulsating stars, Zwintz (2006) restricted her search to stars lying within the classical instability strip.

Based on our experience trying to find fits to the observed frequencies, we note that it is far easier and less ambiguous to fit models for a few well-determined frequencies that are known with confidence to be intrinsic to the star than to try to fit models to a plentitude of frequencies, some of which may or may not be of stellar origin.

Because the PMS models in our grid do not have a well-defined starting point, similar to the ZAMS for post-main-sequence evolution, we are unable to provide an absolute age estimate for the cluster. We start the evolution clocks ticking on the Hayashi track approximately when deuterium burning begins. This is close to but not coincident with the birth line(s) defined by Palla & Stahler (1992, 1993), which are sensitive to the assumed mass-loss rate (not accounted for in our models). Our models can provide an estimate of the relative ages or age spread in the cluster. Our best-fitting model to star 278, constrained by eight modes, has an age of 1.1 Myr, and that to star 278, constrained by six modes, has an age of 0.6 Myr. The best-fit models to the other stars have ages varying from 4 Myr (stars 5 [two modes] and 85 [four modes]) to 8 Myr (star 82 [3 modes]). The ages of the models are, however, very sensitive to the model parameters, such as composition. We feel this is an important area of research, which we hope to address in the future.

In order to move forward, we need spectroscopic measurements of the observed PMS stars in NGC 6530. With reliable effective temperatures, surface gravities, and compositions we can immediately determine whether our modeling is correct.

We have given a small indication of what PMS asteroseismology can do. Of course, our results are tentative and require confirmation. However, this should not be too difficult to achieve. The amplitudes of the oscillations of PMS stars are large enough to be observable from the ground, their spectra appear to be rich enough to provide significant constraints on the models, and their uncomplicated internal structure makes modeling efforts relatively straightforward.

D. B. G. acknowledges the support of the Natural Sciences and Engineering Research Council of Canada. W. W. W. and T. K. acknowledge support by the Austrian Science Funds (P-17580-N02). K. Z. also acknowledges support by the Austrian Science Funds (T334-N16). We made use of the WEBDA database (http://www.univie.ac.at/webda), developed by J.-C. Mermilliod (Laboratory of Astrophysics of the EPFL, Switzerland) and operated by E. Paunzen at the University of Vienna, Austria.

REFERENCES

Alexander, D. R., & Ferguson, J. W. 1994, ApJ, 437, 879
Baglin, A., Auvergne, M., Barge, P., Buey, J.-T., Catala, C., Michel, E., Weiss, W., & COROT Team. 2002, in Proc. First Eddington Workshop, Stellar Structure and Habitable Planet Finding, ed. B. Battrick (ESA SP-485; Noordwijk: ESA), 17
Bahcall, J. N., Pinsonneault, M. H., & Basu, S. 2001, ApJ, 555, 990
Balmforth, N. J. 1992, MNRAS, 255, 603
Breger, M. 1972, ApJ, 171, 539
Brassard, P., Fontaine, G., Bille'res, M., Charpinet, S., Liebert, J., & Saffer, R. A. 2001, ApJ, 563, 1013
Böhm-Vitense, E. 1958, Z. Astrophys., 46, 108
Buzasi, D., Catanzarite, J., Laher, R., Conrow, T. Shupe, D., Gautier, T. N., III, Kreidl, T., & Everett, D. 1999, ApJ, 532, L133
Charpinet, S., Fontaine, G., Brassard, P., Green, E. M., & Chayer, P. 2005, A&A, 437, 575
D'Antona, F., & Mazzitelli, I. 1994, ApJS, 90, 467
Donati, F.-F., Semel, M., Carter, B. D., Rees, D. E., & Cameron, A. C. 1997, MNRAS, 291, 658
Guenther, D. B. 2004, ApJ, 612, 454
Guenther, D. B., & Brown, K. I. T. 2004, ApJ, 600, 419
Guenther, D. B., Demarque, P., Kim, Y.-C., & Pinsonneault, M. H. 1992, ApJ, 387, 372
Guenther, D. B., et al. 2005, ApJ, 635, 547
———. 2007, Commun. Asteroseis., 151, 5
Hayashi, C. 1961, PASJ, 13, 450
Houdek, G., Balmforth, N. J., Christensen-Dalsgaard, J., & Gough, D. O. 1999, A&A, 351, 582
Iben, I., Jr. 1965, ApJ, 141, 993
Iglesias, C. A., & Rogers, F. J. 1996, ApJ, 464, 943
Kilambi, G. C. 1977, MNRAS, 178, 423
Kurtz, D., & Marang, F. 1995, MNRAS, 276, 191
Marconi, M., Ripepe, V., Alcalá, J. M., Covino, E., Palla, F., & Terranegra, L. 2000, A&A, 355, L35
McCall, M. L., Richer, M. G., & Visvanathan, N. 1990, ApJ, 357, 502
Montgomery, M. H., & O'Donoghue, D. 1999, Delta Scuti Star Newsl., 13, 28
Palla, F., & Stahler, S. W. 1992, ApJ, 392, 667
———. 1993, ApJ, 418, 414
Reegen, P. 2007, A&A, 467, 1353
Rogers, F. J. 1986, ApJ, 310, 723
Rogers, F. J., Swenson, F. J., & Iglesias, C. A. 1996, ApJ, 456, 902
Ruoppo, A., Marconi, M., Marques, J. P., Monteiro, M. J. P. F. G., Christensen-Dalsgaard, J., Palla, F., & Ripepi, V. 2007, A&A, 466, 261
Stahler, S. W. 1983, ApJ, 274, 822
Sung, H., Chun, M., & Bessel, M. 2000, AJ, 120, 333
Suran, M., Goupil, M., Baglin, A., Lebreton, Y., & Catala, C. 2001, A&A, 372, 233
Tanner, J. 2006, M.S. thesis, Saint Mary's Univ., Halifax
Tassoul, M. 1980, ApJS, 43, 469
Yi, S. K., Kim, Y.-C., & Demarque, P. 2003, ApJS, 144, 259
Zwintz, K. 2006, Ph.D. thesis, Univ. Vienna
Zwintz, K., Guenther, D. B., & Weiss, W. W. 2007, ApJ, 655, 342 (ZGW07)
Zwintz, K. Marconi, M. Reegen, P., & Weiss, W. W. 2005, MNRAS, 357, 345
Zwintz, K., & Weiss, W. W. 2006, A&A, 457, 237